ISSN 1330–0016
CODEN FIZBE7

THE $\gamma\gamma$-COINCIDENCE MEASUREMENTS OF ^{166}Ho FROM THE (n,γ) REACTION

P. PROKOFJEVS[a], L. I. SIMONOVA[a], M. BALODIS[a], J. BĒRZIŅŠ[a], V. BONDARENKO[a], J. HONZATKO[b], I. TOMANDL[b], S. BONEVA[c], V. A. KHITROV[c] and A. M. SUKHOVOJ[c]

[a] *Nuclear Research Center, LV 2169 Salaspils, Latvia*

[b] *Nuclear Physics Institute, 25068 Řež, Czech Republic*

[c] *Joint Institute of Nuclear Research, 141980 Dubna, Russia*

Received 15 November 1999; Accepted 15 May 2000

Levels of ^{166}Ho were studied using thermal and average resonance neutron capture and with the (d,p) and (d,^{3}He) reactions. We have devoted a large effort to the measurements of the $\gamma\gamma$-coincidence spectra in the broad energy region 50 – 6243 keV. Based on these data and those of earlier studies, the levels are grouped into 23 rotational bands. Among them are 6 new ones. The results are in good agreement with the semiempirical and quasiparticle-phonon model, where Coriolis and residual interactions are taken into account. Details of model interpretation have been presented in a previously published paper.

PACS numbers: 21.10-k, 23.20 Lv, 27.80+w UDC 539.172.4

Keywords: ^{166}Ho levels, (n,γ) reaction, thermal neutrons, Ge spectrometers, $\gamma\gamma$-coincidence spectra

1. *Introduction*

The studies of strongly deformed odd-odd nuclei in the rare-earth region have arisen a considerable interest, both from the theoretical and experimental viewpoints. Theoretically, they offer a unique possibility to obtain information on the proton-neutron residual interaction, by studying the Gallagher-Moszkowski splitting energies of the $\Omega_\mathrm{p} \pm \Omega_\mathrm{n}$ doublets and odd-even energy shifts (Newby shifts) in the $K = 0$ rotational bands. Experimentally, extremely large level density results in complicated spectra of γ-transitions. Because of this, the study of the rare-earth odd-odd nuclei requires the acquisition of large amount of high-quality experimen-

tal data, the time-consuming evaluation of these data and a highly complicated work to develop a level scheme.

A recent example of good new developments of the odd-odd nuclei level schemes is the paper on ^{170}Tm [1]. The ^{166}Ho nucleus resembles ^{170}Tm in some features, however, an expectation of the low-lying vibrational structures increases the actuality for the study of ^{166}Ho.

Most important previous publications on ^{166}Ho include a neutron capture and (d,p) reaction work [2], an ARC experiment [3] with resonance neutrons obtained via boron filter, and a high-precision experiment on high-energy gamma-rays from thermal neutron capture [4]. The most recent Nuclear Data Sheets compilation [5] includes an overview of all previous work, however, this compilation is in some aspects internally contradictory.

A cooperation of several research groups was undertaken to study ^{166}Ho. Reference [6] includes complete tables of the ARC experimental data, as well as those of the (d,p) and (d,^{3}He) reaction measurements, and figures of $\gamma\gamma$-coincidence data. It contains also a detailed analysis of the main experimental and theoretical results on the nuclear structure of ^{166}Ho. Two comparatively long tables of data are published only in the present paper. They contain the $\gamma\gamma$-coincidence spectra from the ^{165}Ho(n,γ)^{166}Ho reaction, measured at the IRT reactor, Salaspils, Latvia, at the Nuclear Physics Institute in Řež, Czech Republic, and at the IBR-30 pulsed reactor, Dubna, Russia.

2. *Experiments and results*

2.1. *The $\gamma\gamma$-coincidence measurements*

The $\gamma\gamma$-coincidence spectra from the ^{165}Ho(n,γ)^{166}Ho reaction were measured at the IRT reactor of the Nuclear Research Center of the Latvian Academy of Sciences. The thermal neutron beam from the tangential experimental channel was transmitted through a 52 cm thick Si filter. The collimated neutron flux (1 cm $\times$ 1 cm) at the target was 5×10^6 n/(cm^2 s). The target material consisting of 0.9 g Ho metal (99% purity) was contained in a thin polyethylene bag. The $\gamma\gamma$-coincidences were recorded using one X-ray Ge-detector (10 cm^3) for the energy range 20 to 465 keV and another one of 78 cm^3 for the energy range 59 to 760 keV. The resolutions (FWHM) of the detectors at 304.6 keV are 1.39 keV and 2.2 keV, respectively. The coincidence resolving time was about 23 ns in a wide energy range of 20 – 1500 keV. The gates were set on the X-ray detector. Two sections of the $\gamma\gamma$-coincidence spectra gated by γ-rays of 116 and 149 keV are shown in Fig. 1.

An additional $\gamma\gamma$-coincidence measurement has been carried out at the Nuclear Physics Institute in Řež, Czech Republic, using large Ge-detectors and a neutron guide facility at the 15 MW light-water LVR-15 reactor. The target consisted of 0.464 g Ho_2O_3 (99.99% purity). The spectra were recorded in the energy range of 100 – 6243 keV with a 22% HPGe and a 12% Ge(Li) detector. The energy

resolutions of the detectors at 1332 keV were 1.9 and 2.1 keV, respectively. More details about the experimental setup and the data acquisition system are given elsewhere [7]. One section of the $\gamma\gamma$-coincidence spectrum for the gate at 239 keV is shown in Fig. 2. The results obtained are summarized in Table 1. This table contains coincident gamma-transitions for 82 gates in the low-energy region, namely, from 54 to 734 keV, and there are 10 gates in the high energy region slightly below neutron binding energy, from 5181 to 5871 keV, also with coincident transitions.

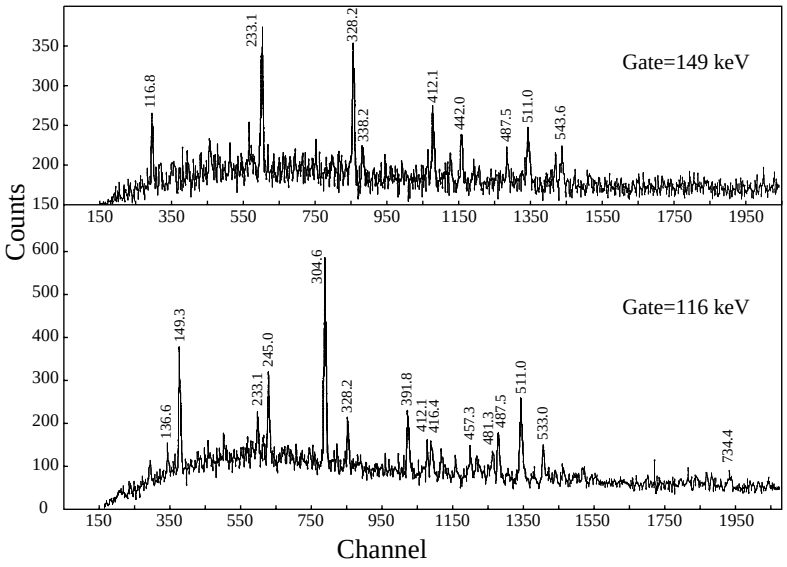

Fig. 1. $\gamma\gamma$-coincidence spectra at the 116 and 149 keV *gates.*

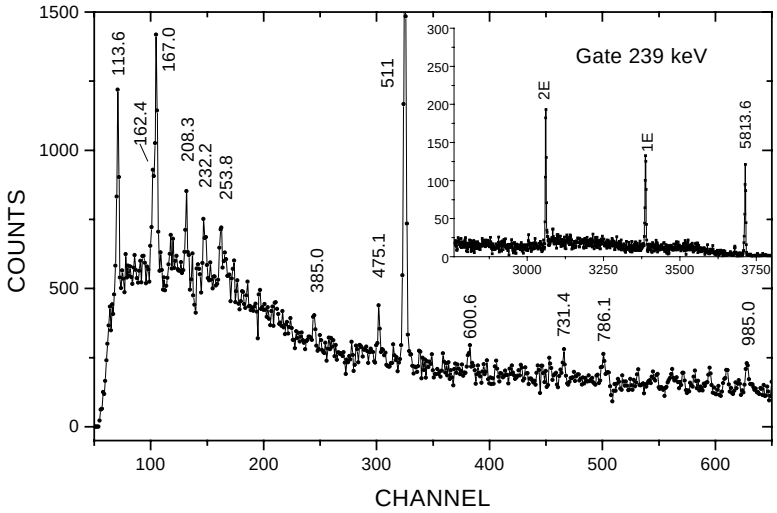

Fig. 2. $\gamma\gamma$-coincidence spectrum at the 239 keV *gate.*

Table 1. Coincident γ-transitions in ^{166}Ho

Gate			Coincident γ-transitions E_γ (keV)
	E_γ (keV)	Placement $E_{\rm in} - E_{\rm fin}$ (keV)	
1	2	3	4
54	54.23	54.23 - 0.0	116.83, 149.30, 233.11, 328.24, 371.75, 391.89, 410.27, 442.00, 457.37, 489.39, 542.86
69	69.76	260.66-190.90	221.17, 287.24, 297.90, 411.09, 509.0
82	82.47	82.47-0.0	290.61, 333.62
87	87.59	348.26-260.66	136.66, 199.71, 306.49, 421.13
	89.59	260.66-171.07	232.28, 509.0
95	94.64	638.22-543.68	543.66
	95.19	693.70-598.51	410.27
	95.95	522.04-426.09	371.75, 425.99
108	108.19	371.98-263.78	442.9
117	116.83	171.07-54.23	149.30, 181.08, 197.33, 233.11, 245.00, 259.6[c], 267.0[c], 304.60, 317.28, 328.24, 391.89, 412.10, 416.47, 426.1[c], 431.8[c], 442.9, 457.37, 463.9, 467.3, 481.31, 487.58, 533.5, 554.3, 577.0, 734.4
126	126.22	180.46-54.23	117.2[c], 149.30, 179.88, 197.33, 231.96, 233.11, 328.24, 412.10, 416.47, 418.08, 487.58, 538.4, 579.9[c]
140	140.11	683.81-543.68	489.39, 543.66
	141.59	567.65-426.09	371.75, 425.99
149	149.30	329.77-180.46	116.83, 126.22, 179.88, 233.11, 268.15, 328.24, 338.20, 412.10, 430.31, 442.17[c] , 453.82, 458.74[c], 489.03[c], 538.6[c], 545.11[c], 680.11[c], 689.19[c], 1009.0[c]
157	157.34	348.26-190.90	199.71, 421.13, 423.37
163	163.35	760.37-597.02	116.83, 239.14, 304.60, 416.47, 542.86
167	166.98	597.02-430.04	239.14, 848.97[c]
	167.45	431.24-263.78	
170	169.71	837.73-668.01	116.83, 487.58, 543.66, 613.63[c]
	170.58	543.68-373.15	290.61
179	179.03	605.10-426.09	371.75, 425.99
	179.88	557.69-377.80	116.71, 149.30
		595.84-416.01	245.00, 333.62
181	180.54	634.3-453.7	98.20, 105.51
	181.08	371.98-190.90	186.87, 779.82[c], 789.1[c]
	182.30	658.08-475.73	304.60
186	186.14	668.01-481.85	169.71
	186.58	558.57-371.98	108.19, 111.32, 181.08
193	192.33	668.01-475.73	304.60
	193.10	453.77-260.66	123.43, 180.54, 488.4[c]
195	194.52	567.65-373.15	116.83, 290.61
	195.68	792.98-597.02	149.30, 542.86
197	197.33	377.80-180.46	116.83, 126.68, 179.88
	197.67	662.23-464.55	181.08, 239.14, 371.75, 410.27, 425.99
199	198.31	628.43-430.04	239.14, 371.75, 425.99
	199.71	547.93-348.26	116.83, 149.30, 157.34, 209.69, 267.19, 289.52[c]
208	208.34	638.22-430.04	239.14, 425.99
	208.90	807.33-598.51	116.83, 149.30, 304.60, 425.99, 542.86

Table 1. (continued)

1	2	3	4
210	209.69	757.58-547.93	181.08, 221.17
	210.30	558.57-348.26	232.29, 256.60
			289.8[c]
214	214.44	736.49-522.04	371.75, 410.27, 425.99
221	221.17	481.85-260.66	186.15, 232.28, 242.90, 256.60, 267.19,
			289.07[c], 322.2[c], 932.76[c]
	222.63	815.07-592.46	331.88, 401.56
232	231.95	605.10-373.15	290.61
	232.28	662.23-430.04	239.14
			180.03[c]
233	233.11	562.85-329.77	116.83, 126.22, 149.30
	233.79	832.26-598.51	371.75, 410.27, 425.99
	234.79	529.81-295.08	289.12
239	239.14	430.04-190.90	113.64, 162.45, 166.98, 186.15, 208.34, 232.28, 253.78,
			385.0, 475.14[c], 600.6[c], 731.4[c], 786.1[c], 985.0[c]
245	245.00	416.01-171.07	116.83, 146.80, 152.71, 163.35, 179.88, 181.08, 188.98,
			246.07, 257.82, 288.60
	246.07	662.23-416.01	245.00, 290.61, 333.62
			277.7[c]
254	253.78	683.81-430.04	239.14
			289.42[c], 411.00[c]
256	255.37	628.43-373.15	290.61
	256.60	815.07-558.57	181.08, 186.58, 221.17, 297.90
258	257.81	263.78-5.97	108.19, 167.45, 455.60
260	260.75	736.49-475.73	116.83, 290.61, 304.60
264	262.93	925.51-662.23	246.07
	263.36	558.57-295.08	289.12
	265.12	638.22-373.15	290.61
267	266.53	742.09-475.73	245.00, 290.61, 304.60, 333.62
	267.19	815.07-547.93	199.71, 221.17
	267.82	683.81-416.01	116.83, 245.00, 290.61, 333.62
289	288.60	704.94-416.01	245.00, 333.62
	289.12	295.08-5.97	128.56, 150.27, 234.79, 426.89[c], 553.37[c]
291	290.61	373.15-82.47	170.58, 188.98, 194.52, 231.96, 255.37, 260.75, 265.12,
			352.28, 401.31[c], 635.7[c], 658.9[c], 688.5[c], 711.8[c], 970.7[c]
298	297.90	558.57-260.66	232.28, 256.60
305	304.60	475.73-171.07	116.83, 129.35, 182.30, 192.33, 260.75, 266.53, 317.28,
			392.2[c], 404.7[c], 585.97[c], 686.28[c]
311	309.59	725.58-416.01	333.62
	312.90	905.60-592.46	331.88, 401.56
317	317.28	792.98-475.73	116.83, 304.60
328	328.24	658.08-329.77	116.83, 126.22, 149.30
			267.9[c]
334	333.62	416.01-82.47	146.80, 151.53, 181.08, 182.30, 188.98, 219.44, 246.07,
			267.82, 288.60, 309.59, 357.04, 376.91
338	338.20	668.01-329.77	149.30
348	347.24	719.44-371.98	108.19, 111.32, 181.08
353	352.28	725.58-373.15	290.61
372	371.75	426.09-54.23	116.19, 140.54, 141.59, 173.47, 179.03, 197.67, 214.44,

Table 1. (continued)

1	2	3	4
372			233.79, 388.82, 534.9
392	391.89	562.85-171.07	116.83, 313.48
395	394.5	870.14-475.73	304.60
402	401.31[c]	774.51-373.15	290.61
	401.56	592.46-190.90	222.63, 282.60, 312.90
			310.89, 332.53[c], 427.14[c]
407	406.83	736.49-329.77	116.83, 149.30, 158.70
412	410.27	464.55-54.23	197.67, 214.44
	412.1	592.46-180.46	116.83, 126.22
	412.1	742.09-329.77	116.83, 126.22, 149.30
416	416.47	597.02-180.46	116.83, 163.35
426	425.99	426.09-0.0	141.59, 179.03, 197.67, 214.44, 233.79
	426.89[c]	722.00-295.08	289.12
	427.0	598.51-171.07	116.83, 163.35
			401.56
431	430.31	760.37-329.77	116.83, 149.30
434	433.92	605.10-171.07	116.83
		1030.47-597.02	149.30, 181.08, 221.17, 239.14, 290.61, 304.60, 333.62, 371.75, 401.56, 425.99, 489.39, 542.86, 543.66
443	442.0	1161.30-719.44	
	442.17[c]	771.77-329.77	
	442.9	815.07-371.98	108.19, 181.08
455	454.96	832.26-377.80	116.83, 149.30
	455.60	719.44-263.78	442.0
			205.99
457	457.37	628.43-171.07	116.83
			134.5, 149.30
464	463.9	654.80-190.90	117.26
467	467.3	638.22-171.07	116.83
477	477.4	658.08-180.46	116.83
			425.99, 542.86
481	481.3	742.08-260.66	
			116.83, 425.99
488	487.58	668.01-180.46	116.83, 126.22, 169.71
	489.39	543.68-54.23	140.11, 163.35, 182.04
	489.03[c]	819.12-329.77	116.83, 149.30
			543.66, 549.70
509	509.0	562.85-54.23	
		1030.47-522.04	341.57
533	533.5	704.94-171.07	116.83
535	534.9	961.05-426.09	371.75, 425.99
538	538.4	868.27-329.77	116.83, 149.30
		1130.98-592.46	181.08, 221.17, 239.14, 304.60, 371.75, 401.56, 410.27, 425.99, 489.39, 543.66
			233.79, 289.85
543	542.86	597.02-54.23	145.00, 163.35, 169.71
	543.66	543.68-0.0	140.11, 163.35
	543.89[c]	873.66-329.77	116.83, 149.30

Table 1. (continued)

1	2	3	4
546	546.9[c]	876.63-329.77	116.83, 149.30
551	550.5	880.61-329.77	116.83, 149.30
554	553.37[c]	848.49-295.08	289.12
	554.3	725.58-171.07	116.83
		815.07-260.66	
		884.05-329.77	116.83, 149.30
577	577.0	757.58-180.46	116.83, 126.22
			104.29
586	585.6	1061.7-475.73	116.83, 304.60
591	589.4	1135.0-543.68	116.83, 149.30, 166.98, 239.14, 290.61,
			489.39, 543.66
	593.8	1190.1-597.02	
601	600.8	1030.47-430.04	239.14
681	681.7	1010.7-329.77	116.83, 149.30
685	686.28[c]	1161.4-475.73	116.83, 304.60
688	688.51	1061.4-373.15	290.61
700	701.1[c]	1030.47-329.77	116.83, 149.30
714	714.7[c]	885.39-171.07	116.83
		905.60-190.90	
734	733.9[c]	905.60-171.07	116.83
5181	5181.84	6243.69-1061.85	221.17, 304.60, 333.62
5338	5338.30	6243.69-905.60	714.7[c]
5428	5428.47	6243.69-815.07	222.63, 256.60, 267.19, 350.61, 385.0, 388.8[c],
			442.9, 624.0
5473	5473.82	6243.69-769.54	509.0
5524	5524.21	6243.69-719.44	455.60
5685	5685.01	6243.69-558.57	186.58, 297.90
5761	5761.72	6243.63-481.85	221.17
5767	5767.92	6243.63-475.73	304.60
5813	5813.55	6243.63-430.04	239.14
5871	5871.54	6243.63-373.15	290.61
		6243.63-371.98	181.08

[c]the transition energy from coincidence data

2.2. Two-step cascades in the (n, γ) reaction

The coincidence technique with the pulse-amplitude summation of two-step cascades following thermal neutron capture is a source of information about the high-energy and low-energy γ-ray coincidences. Measurements were performed at the IBR-30 pulsed reactor in JINR, Dubna, Russia. Thermal neutron capture was selected by the time-of-flight method. The ^{165}Ho target mass was 4 g. Data acquisition took about 400 h. The spectrometer consisted of a 15% efficient HPGe detector and a 10% efficient Ge(Li) detector with 3-4 keV energy resolution at 1332 keV. The time resolution was 10 to 12 ns with a ^{60}Co source. To avoid the backscattered gamma quanta, a 2.5 g/cm^2 thick lead filter was used. The experimental method

and processing procedure have already been described [8,9]. The data processing included the off-line construction of spectra of coincidence pulses after summation of their amplitudes. This spectrum (Fig. 3) has peaks, corresponding to all two-step gamma cascades between the compound state and certain low-lying levels. Events selected in each peak in Fig. 3 represent the distribution for two-step cascades which de-excite the compound state via many intermediate states to a certain final level (Fig. 4). The results of these $\gamma\gamma$-coincidence measurements are listed in Table 2.

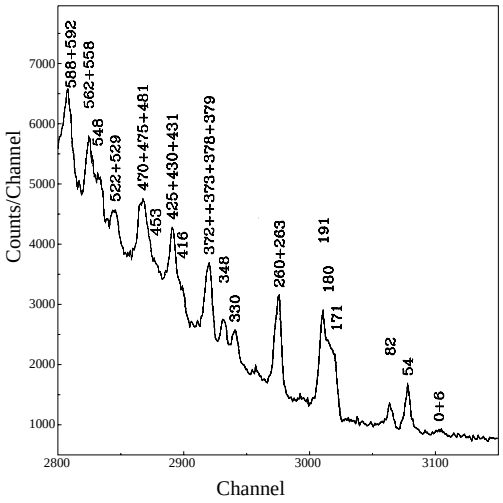

Fig. 3. A part of the spectrum of coincident pulses after their amplitude summation in the high-energy – low-energy region.

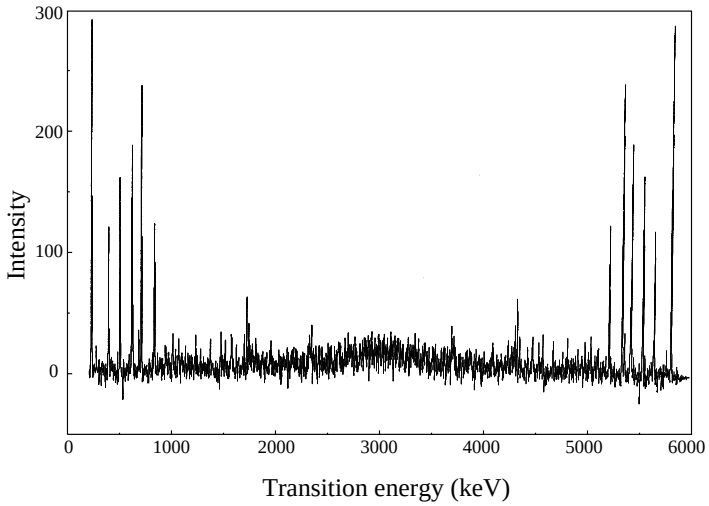

Fig. 4. Spectrum of γ-rays with the condition that the two-step γ-ray cascades go to the level at 190.9 keV.

Table 2. A list of energies E_1 and E_2 of measured cascade transitions and their relative intensities $i_{\gamma\gamma} \pm \Delta i_{\gamma\gamma}$ in percent of the total intensity of the two-step cascades which have the same total energy. $E_M \pm \Delta E_M$ is the intermediate level energy for $E_M < 1200$ keV. E_f is the energy of the final levels of the cascades.

Legend: (1) – E_1 (keV), (2) – E_2 (keV), (3) – $i_{\gamma\gamma}(\Delta i_{\gamma\gamma})$, (4) – $E_M(\Delta E_M)$ (keV)

(1)	(2)	(3)	(4)
$E_1 + E_2 = 6242.7$ keV; $E_f = 0$ keV			
5698.9	543.8(7)	5.0(15)	543.0(8)
5527.3	715.4(8)	3.3(11)	717.0(14)
5206.5	1036.2(8)	3.5(3)	1035.8(6)
$E_1 + E_2 = 6188.4$ keV; $E_f = 54.3$ keV			
5767.9	420.5(6)	0.5(2)	475.9(12)
5700.4	488.0(8)	0.3(1)	543.0(8)
5680.3	508.2(8)	0.3(1)	563.7(11)
5645.4	543.1(4)	1.0(2)	599.5(18)
5591.9	596.6(6)	0.4(1)	651.5(8)
5574.6	613.9(6)	0.5(1)	668.3(4)
5372.4	816.1(4)	1.0(2)	873.6(24)
5361.5	826.9(3)	2.0(3)	881.9(9)
5296.1	892.4(5)	1.3(3)	947.1(6)
5290.4	898.1(10)	0.4(2)	953.4(11)
5267.3	921.1(9)	0.3(1)	973.7(18)
5238.4	950.0(4)	2.5(5)	1004.9(9)
5227.2	961.2(5)	1.6(3)	1014.6(19)
5213.1	975.4(6)	0.8(2)	1030.2(7)
5206.8	981.6(9)	0.4(2)	1035.8(6)
5188.8	999.6(11)	0.3(1)	1053.9(7)
5179.9	1008.5(4)	1.1(2)	1062.7(9)
5154.2	1034.3(7)	0.5(2)	1087.8(10)
5089.4	1099.0(5)	0.8(2)	1155.5(27)
$E_1 + E_2 = 6160.1$ keV; $E_f = 82.6$ keV			
5370.1	790.0(10)	0.5(2)	873.6(24)
5361.8	798.3(4)	3.0(5)	881.9(9)
5354.8	805.4(7)	1.2(3)	891.2(46)
5284.3	875.9(9)	0.5(2)	960.3(18)
5270.9	889.2(10)	0.5(2)	973.7(18)
5212.4	947.7(2)	13.5(13)	1030.2(7)
5207.8	952.4(9)	1.9(8)	1035.8(6)
5180.9	979.3(7)	0.9(3)	1062.7(9)
5564.0	596.1(9)	0.7(3)	
5386.3	773.8(11)	0.5(2)	
$E_1 + E_2 = 6071.6$ keV; $E_f = 171.1$ keV			
5765.6	304.2(2)	2.5(3)	475.9(12)
5678.1	391.6(6)	0.4(1)	563.7(11)
5643.1	426.7(4)	0.9(2)	599.5(18)
5360.9	708.9(6)	0.5(1)	881.9(9)
5355.1	714.7(5)	0.7(2)	891.2(46)
5337.2	734.4(3)	0.6(1)	906.1(6)
5294.9	774.9(3)	0.7(1)	947.1(6)
5231.7	838.1(6)	0.5(1)	1010.5(6)
5212.5	857.3(4)	0.9(2)	1030.2(7)
5153.7	916.1(7)	0.4(1)	1087.8(10)
5126.6	943.2(9)	0.4(1)	1115.3(12)
5120.6	949.2(6)	0.6(2)	1121.2(7)
5086.5	983.3(6)	0.6(2)	1155.5(27)

(1)	(2)	(3)	(4)
$E_1 + E_2 = 6071.6$ keV; $E_f = 171.1$ keV (*continued*)			
5080.2	989.6(3)	1.5(3)	1161.7(12)
5179.0	892.6(6)	0.5(1)	
$E_1 + E_2 = 6062.2$ keV; $E_f = 180.5$ keV			
5758.5	303.6(5)	0.5(1)	483.1(11)
5648.0	414.0(6)	0.3(1)	593.8(7)
5640.3	421.7(7)	0.3(1)	599.5(18)
5584.5	477.5(7)	0.3(1)	658.1(5)
5574.0	488.0(5)	0.3(1)	668.3(4)
5483.9	578.1(7)	0.3(1)	757.7(10)
5433.6	628.4(8)	0.4(2)	807.9(20)
5409.7	652.2(7)	0.3(1)	832.7(12)
5369.6	692.4(7)	0.3(1)	873.6(24)
5345.9	716.1(7)	0.8(3)	891.2(46)
5237.7	824.3(4)	1.0(2)	1004.9(9)
5219.2	842.8(7)	0.3(1)	1023.3(7)
5212.8	849.2(7)	0.4(1)	1030.2(7)
5180.9	881.1(9)	0.5(2)	1062.7(9)
5155.1	906.9(7)	0.4(1)	1087.8(10)
5122.0	940.0(6)	0.8(2)	1121.2(7)
5110.6	951.4(12)	0.4(1)	1134.3(15)
5104.4	957.4(3)	1.4(2)	1137.9(5)
5081.2	981.0(7)	0.5(1)	1161.5(10)
5656.5	405.4(6)	0.4(1)	
5635.1	426.8(12)	0.2(1)	
5116.3	945.4(13)	0.5(2)	
$E_1 + E_2 = 6051.0$ keV; $E_f = 191.7$ keV			
5812.5	238.5(1)	5.7(4)	430.2(10)
5649.5	401.5(2)	2.3(3)	593.8(7)
5642.2	408.8(6)	0.5(1)	599.5(18)
5559.4	491.6(7)	0.3(1)	683.3(15)
5452.6	598.4(7)	0.2(1)	790.1(20)
5426.9	624.1(1)	3.9(3)	816.0(10)
5417.8	633.2(3)	1.4(2)	826.1(16)
5360.8	690.2(4)	0.7(2)	881.9(9)
5342.4	708.6(10)	0.3(2)	891.2(46)
5336.7	714.3(1)	5.1(4)	906.0(10)
5225.9	825.1(11)	0.2(1)	1014.6(19)
5219.7	831.3(12)	0.2(1)	1023.3(7)
5212.1	838.9(7)	2.2(9)	1030.2(7)
5179.2	871.8(9)	0.2(1)	1062.7(9)
5157.0	894.0(9)	0.2(1)	1087.8(10)
5108.8	942.2(7)	0.3(1)	1134.3(15)
5100.7	950.3(6)	0.4(1)	1143.4(16)
5092.0	959.0(7)	0.3(1)	1155.5(27)
5074.1	976.9(7)	0.4(1)	1166.2(18)
5534.6	516.4(7)	0.5(2)	

Table 2. (continued)

Legend: (1) – E_1 (keV), (2) – E_2 (keV), (3) – $i_{\gamma\gamma}(\Delta i_{\gamma\gamma})$, (4) – $E_M(\Delta E_M)$ (keV)

(1)	(2)	(3)	(4)
$E_1 + E_2 = 5980.6$ keV; $E_f = 262.1$ keV			
5760.6	220.1(4)	0.6(1)	483.1(11)
5524.7	456.0(1)	7.1(5)	717.0(14)
5435.3	545.4(5)	0.5(1)	807.9(20)
5426.2	554.4(3)	1.1(2)	816.0(10)
5417.4	563.3(5)	0.5(1)	826.1(16)
5366.0	614.6(9)	0.3(1)	873.6(24)
5360.1	620.5(7)	0.6(2)	881.9(9)
5354.0	626.6(7)	0.4(1)	891.2(46)
5280.5	700.1(3)	1.3(2)	960.3(18)
5244.5	736.1(10)	0.2(1)	996.8(8)
5215.3	765.3(11)	0.4(2)	1029.0(12)
5210.7	769.9(4)	1.4(3)	1030.2(7)
5182.6	798.1(9)	0.2(1)	1060.8(6)
5153.8	826.8(9)	0.3(1)	1087.8(10)
5143.9	836.8(8)	0.3(1)	1099.8(11)
5127.0	853.7(3)	2.5(3)	1115.3(12)
5106.7	873.9(6)	0.8(2)	1134.3(15)
5088.5	892.1(8)	0.4(2)	1155.5(27)
5081.9	898.8(5)	1.0(2)	1161.7(12)
5051.9	928.7(5)	0.8(2)	1189.9(11)
$E_1 + E_2 = 5912.8$ keV; $E_f = 329.9$ keV			
5584.6	328.2(4)	1.3(3)	658.1(5)
5543.1	369.6(10)	0.7(3)	701.5(16)
5485.9	426.9(9)	0.6(3)	757.7(10)
5433.5	479.2(11)	0.4(2)	807.9(20)
5427.5	485.2(10)	0.5(2)	816.0(10)
5366.1	546.6(5)	1.5(3)	873.6(24)
5288.2	624.6(10)	0.5(2)	953.4(11)
5232.8	679.9(8)	0.7(2)	1010.5(6)
5211.9	700.8(4)	1.7(3)	1030.2(7)
5178.7	734.0(7)	0.6(2)	1062.7(9)
5120.9	791.9(11)	0.5(2)	1121.2(7)
5096.5	816.2(10)	0.5(2)	1143.4(16)
5087.3	825.5(11)	0.5(2)	1155.5(27)
5081.4	831.3(7)	1.1(3)	1161.7(12)
$E_1 + E_2 = 5894.3$ keV; $E_f = 348.4$ keV			
5590.2	304.1(7)	0.8(3)	651.5(8)
5472.4	421.9(5)	1.9(5)	770.3(7)
5348.6	545.7(6)	1.2(4)	891.2(46)
5213.2	681.1(6)	1.1(3)	1030.2(7)
5178.3	716.0(7)	1.0(3)	1062.7(9)
5141.2	753.1(10)	0.6(3)	1099.8(11)
5128.4	765.9(3)	3.2(5)	1115.3(12)
5087.8	806.5(7)	0.8(3)	1155.5(27)
5080.9	813.3(6)	1.0(3)	1161.7(12)

(1)	(2)	(3)	(4)
$E_1 + E_2 = 5870.6$ keV; $E_f = 372.1$ keV			
5523.0	347.6(7)	0.8(3)	719.7(15)
5437.5	433.1(8)	0.3(1)	807.9(20)
5428.0	442.6(2)	2.4(3)	816.0(10)
5414.3	456.3(4)	0.7(2)	826.1(16)
5359.1	511.5(2)	4.9(5)	881.9(9)
5351.6	519.0(7)	0.6(2)	891.2(46)
5246.4	624.2(5)	0.6(2)	996.8(8)
5236.3	634.3(8)	0.3(1)	1004.9(9)
5213.1	657.5(4)	0.9(2)	1030.2(7)
5206.3	664.3(8)	0.4(1)	1035.8(6)
5181.5	689.1(1)	5.3(4)	1060.8(6)
5155.0	715.6(3)	1.0(2)	1087.8(10)
5127.5	743.1(10)	0.2(1)	1115.3(12)
5109.1	761.5(6)	0.4(1)	1134.3(15)
5083.5	787.1(4)	1.4(3)	1155.5(27)
5078.8	791.8(7)	0.8(2)	1166.2(18)
5443.4	427.4(9)	0.8(2)	
$E_1 + E_2 = 5826.5$ keV; $E_f = 416.2$ keV			
5431.7	394.8(9)	0.9(3)	807.9(20)
5425.1	401.4(2)	5.8(8)	816.0(10)
5283.9	542.6(7)	1.0(3)	960.3(18)
5230.4	596.1(7)	1.0(3)	1014.6(19)
5212.0	614.5(4)	1.9(4)	1030.2(7)
5180.4	646.1(2)	7.3(9)	1062.7(9)
5122.1	704.4(9)	0.8(3)	1121.2(7)
$E_1 + E_2 = 5812.6$ keV; $E_f = 430.1$ keV			
5213.2	599.5(4)	2.6(5)	1029.0(12)
5080.5	732.1(5)	1.8(4)	1161.7(12)
$E_1 + E_2 = 5788.8$ keV; $E_f = 453.9$ keV			
5245.4	543.5(10)	1.2(5)	996.8(8)
5127.6	661.3(2)	14.5(15)	1115.3(12)
5087.1	701.7(9)	1.2(5)	1155.5(27)
5075.2	713.6(6)	2.4(6)	1166.2(18)
$E_1 + E_2 = 5766.6$ keV; $E_f = 476.1$ keV			
5213.8	552.6(9)	0.6(3)	1028.7(15)
5180.4	586.1(2)	4.0(5)	1062.7(9)
5143.0	623.6(8)	0.5(2)	1099.8(11)
5083.2	683.4(4)	1.8(3)	1155.5(27)
5077.4	689.1(5)	1.4(3)	1166.2(18)
5054.0	712.6(7)	0.5(2)	1189.9(11)
5173.5	593.1(9)	0.5(2)	
$E_1 + E_2 = 5720.5$ keV; $E_f = 522.2$ keV			
5124.6	595.9(14)	0.8(4)	1115.3(12)
$E_1 + E_2 = 5694.6$ keV; $E_f = 548.1$ keV			
5127.1	567.5(5)	1.6(5)	1115.3(12)
5081.9	612.7(6)	1.5(4)	1161.7(12)

The transitions listed in Table 2 are limited to those two-step cascades which finish at the following final levels (0, 54.3, 82.6, 171.1, 180.5, 191.7, 262.1, 329.9, 348.4, 372.1, 416.2, 430.1, 453.9, 476.1, 522.2 and 548.1 keV). The spin difference between the initial and final level of detected cascades is $|J_\lambda - J_f| \leq 2$. Only $E1$, $M1$ and

$E2$ transitions were detected. Cascade intensities were normalized so that the area of the experimental distribution in the interval 520 keV $\leq E_\gamma \leq$ ($E_{\rm cascade}$ − 520 keV) was 100% for each level where $E_{\rm cascade} = E_1 + E_2 = B_n - E_{\rm final}$. There are several cascade transitions with $E_\gamma \leq 520$ keV and their intensities, presented in the Table 2, have reduced values taking into account the experimental conditions.

3. Discussion

In Ref. [6], one can find a detailed interpretation and analysis of the level scheme, based on the previous data and on our new experimental and theoretical results. In Table 3, we present an account of the partial level scheme including levels of several new or significantly changed rotational bands. An important role of the coincidence measurements is illustrated in this Table.

Table 3. Level depopulation for several rotational bands of ^{166}Ho.

I^π	$E_{lev}(\Delta E)$	$E_\gamma(\Delta E)$	$I_\gamma(\Delta I)$	Mult.	E_f	I^π
1	2	3	4	5	6	7
5^- $\{(7/2^-[523] + 7/2^+[633])$ -$Q_{22}\}$						
5^-	431.240(5)	425.30(3)	1.3(3)		5.97	7^-
		167.450(5)^c	0.95(9)	E1	263.78	5^+
6^-	529.817(8)	524.2(3)	0.5(1)		5.97	7^-
		266.03(5)^c	0.28(3)		263.78	5^+
		234.79(5)^c	0.05(1)		295.08	6^+
		150.268(8)^c	0.11(2)		379.54	6^+
		98.572(16)	0.04(1)		431.24	5^-
7^-	644.29(6)	506.8(3)	0.20(4)		137.73	8^-
		213.04(6)	0.010(2)		431.24	5^-
		114.50(3)^w	0.010(2)		529.81	6^-
2^- $(3/2^+[411] + 1/2^-[521])$						
2^-	638.229(9)	467.3(3)^c	0.30(10)		171.07	3^-
		265.12(5)^c	0.18(4)		373.15	1^-
		208.34(4)^c	0.065(10)		430.04	2^+
		173.47(12)^c	0.020(4)		464.55	2^+
		116.197(13)^c	0.06(1)		522.04	3^+
		94.643(11)^c	0.20(3)		543.68	2^-
3^-	704.947(9)	533.5(3)^c	0.60(20)		171.07	3^-
		288.60(7)^c	0.12(2)		416.01	2^-
		274.77(7)^c	0.13(3)		430.04	2^+
		229.00(7)^w	0.05(2)		475.73	3^-
		161.42(2)	0.030(4)		543.68	2^-
		107.71(3)	0.030(8)		597.02	3^-
		109.241(12)	0.030(6)		595.84	1^-
		99.584(16)	0.020(5)		605.10	2^+

Table 3. (continued)

1	2	3	4	5	6	7
2^- $(3/2^+[411]+1/2^-[521])$ (*cont.*)						
4^-	792.98(2)	612.0(5)	0.30(6)		180.46	4^-
		376.91(14)^c	0.12(2)		416.01	2^-
		317.28(3)^c	0.22(4)		475.73	3^-
		230.11(5)^w	0.030(6)		562.85	4^-
		195.687(14)^c	0.08(1)		597.02	3^-
		154.71(3)	0.025(5)		638.22	2^-
6^+ $(7/2^-[523]+5/2^-[512])$						
6^+	295.088(9)	289.120(15)^c	2.3(2)	E1	5.97	7^-
7^+	423.654(10)	285.81(8)	0.06(2)		137.73	8^-
		159.89(3)	0.010(1)		263.78	5^+
		128.566(5)^c	0.14(2)		295.08	6^+
$6^+(7/2^-[523]+5/2^-[523])$						
6^+	722.00(15)	426.89(15)^c	0.13(4)^b		295.08	6^+
7^+	848.49(21)	553.37(21)^c	0.07(2)^b		295.08	6^+
$2^+(7/2^-[523]-3/2^-[521])$						
2^+	905.60(1)	733.94(21)^{c,s}	0.024(7)		171.07	3^-
		714.7(2)^{c,s}	0.26(8)		190.90	3^+
		475.8(3)^c	0.15(3)		430.04	2^+
		312.90(8)^c	0.12(6)		592.46	3^+
		145.228(7)	0.140(14)		760.37	3^-
3^+	961.23(16)	700.8(3)^s	0.06(2)		260.66	4^+
		542.8(8)^s	0.006(2)		416.01	2^-
		534.9(4)^c	0.30(6)		426.09	1^+
4^+	1030.47(23)	858.0(5)^{c,s}	0.04(1)		171.07	3^-
		849.5(7)^s	0.015(5)		180.46	4^-
		839.9(7)^s	0.13(4)		190.90	3^+
		770.5(4)^s	0.06(2)		260.66	4^+
		701.1(5)^{c,s}	0.016(5)		329.77	5^-
		600.8(7)^{c,s}	0.024(6)		430.04	2^+

[a]Transition not observed; placement suggested by $\gamma\gamma$-coincidence data
[b]I_γ estimated by taking into account coincidence data
[c]Low-energy $\gamma\gamma$-coincidence
[d]Doublet
s High-energy $\gamma\gamma$-coincidence
[t]γ-transition intermediate between coincident $\gamma\gamma$-transitions
[w]Multiply placed γ-transition

Reference [6] contains the discussion of 23 bands based on the semiempirical rotation-vibration-particle model. Two of them: 431.24 keV 5^-, and 543.68 keV 2^-, include appreciable γ-vibrational $|K_0-2|$ components based on the 7^- and 0^-

bands, having as the band heads, respectively, the 5.9 keV level and the ground state, with the configuration $p7/2^-[523] \pm n7/2^+[633]$.

Eleven Gallagher-Moszkowski splitting energies and two Newby shifts could be determined. An analysis based on the quasiparticle-phonon model (QPM) calculations is given in Ref. [6]. These calculations take into account Coriolis and residual interactions, as well as quadrupole and octupole phonon excitations.

A few earlier proposed bands have not been confirmed, namely, the 350 keV 1^-, 525 keV 0^- [10], 803 keV 0^+, 721 keV 3^+ and 891 keV 4^+ bands [11].

4. Conclusions

Reference [6], together with the present paper, collects the results of a larger collaboration devoted to the study of ^{166}Ho nuclear structure.

It is clearly shown, that the ^{166}Ho is the best suited odd-odd nucleus in the rare-earth strongly-deformed region where the most low-lying γ-vibration states can be identified. 93 levels grouped into 23 bands are discussed in Ref. [6], and six of these bands can be considered as entirely new.

In the present paper, two comparatively long tables of the $\gamma\gamma$-coincidence measurements of the ^{165}Ho(n,γ)^{166}Ho reaction are given. Some of these data play a crucial role, establishing a reliable and internally consistent level scheme.

Acknowledgements

We thank our colleagues who participated in the large holmium collaboration: H. F. Wirth, T. von Egidy, C. Doll, J. Ott, W. Schauer, R. W. Hoff, R. L. Gill, R. F. Casten, D. G. Burke, J. Kvasil and A. Macková. Their results are included in the earlier published paper, and they have made fruitful contributions for a better knowledge of the ^{166}Ho structure. This work was partially supported by RFBR Grant No. 99-02-17863.

The Riga group thanks to Tamāra Krasta for editing the manuscript.

References

[1] R. W. Hoff, H. G. Börner, K. Schreckenbach, G. G. Colvin, F. Hoyler, W. Schauer, T. von Egidy, R. Georgii, J. Ott, S. Schründer, R. F. Casten, K. L. Gill, M. Balodis, P. Prokofjevs, L. Simonova, J. Kern, V. A. Khitrov, A. M. Sukhovoj, G. Bersillon, S. Joly, G. Graw, D. Hofer and B. Valmon, Phys. Rev. C **54** (1996) 78.

[2] H. T. Motz, E. Jurney, O. W. B.Schult, H. R. Koch, U. Gruber, B. P. Maier, H. Baader, G. L. Struble, J. Kern, R. K. Sheline, T. von Egidy, Th. Elze, E. Bieber and A. Bäcklin, Phys. Rev. **155** (1967) 1265.

[3] L. M. Bollinger and G. E. Thomas, Phys. Rev. C **2** (1970) 1951.

[4] T. J. Kennet, M. A. Islam and W. V. Prestwich, Phys. Rev. C **30** (1984) 1840.

[5] E. N. Shurshikov and N. V. Timofeev, Nucl. Data Sheets **67** (1992) 53.

[6] P. Prokofjevs, L. I. Simonova, M. Balodis, J. Bērziņš, V. Bondarenko, H. F. Wirth, T. von Egidy, C. Doll, J. Ott, W. Schauer, R. W. Hoff, R. F. Casten, R. L. Gill, J. Honzátko, I. Tomandl, S. Boneva, V. A. Khitrov, A. M. Sukhovoj, D. G. Burke, J. Kvasil and A. Macková, Phys. Rev. C **61** (2000) 044305, 1.

[7] J. Honzátko, K. Konečný, I. Tomandl, J. Vacik, F. Bečvář and P. Cejnar, Nucl. Instr. and Methods A **376** (1996) 434.

[8] S. T. Boneva, E. V. Vasilieva, Yu. P. Popov, A. M. Sukhovoj and V. A. Khitrov, Sov. J. Part. Nucl. **22** (1991) 232.

[9] A. M. Sukhovoj and A. M. Khitrov, Instr. Exp. Tech. (USSR) **27** (1984) 1071.

[10] R. K. Sheline and P. C. Sood, Phys. Rev. C **40** (1989) 1065.

[11] R. A. Dewberry, R. K. Sheline, R. G. Lanier and R. Lasijo, Z. Phys. A **307** (1982) 351.

SUDESNA MJERENJA $\gamma\gamma$-RASPADA STANJA ^{166}Ho NASTALIH REAKCIJOM (n,γ)

Proučavali smo stanja ^{166}Ho nastala termičkim i prosječnim rezonantnim uhvatom neutrona, te (d,p) i (d,^{3}He) reakcijama. Uložili smo velik trud u mjerenjima sudesnih $\gamma\gamma$-spektara u širokom energijskom području od 50 do 6243 keV. Na osnovi tih i ranijih podataka, stanja su grupirana u 23 rotacijske vrpce. Među njima je i 6 novih. Ishodi su u suglasju s poluempiričkim i kvazičestično-fononskim modelom, uzimajući u obzir Coriolisovo međudjelovanje i rezidualne interakcije. Podrobnosti modelskog tumačenja objavljene u u ranijem članku.